Journal of Drug Delivery Science and Technology 74 (2022) 103608

Contents lists available at ScienceDirect

Journal of Drug Delivery Science and Technology

journal homepage: www.elsevier.com/locate/jddst

Inhibition of metastatic bone cancer with a cascade targeting of docetaxel

Liang Wei [a,b,c,d], Dong Zhang [a,b,c,d], Bin Xiong [a,b,c,d], Siyan Zhang [a,b,c,d], Yuangang Zu [a,b,**], Shougang Jiang [a,b,c,d,*]

[a] Key Laboratory of Forest Plant Ecology, Ministry of Education, Northeast Forestry University, Harbin, PR China
[b] State Engineering Laboratory of Bio-Resources Eco-Utilization, Northeast Forestry University, Harbin, PR China
[c] College of Chemistry Chemical Engineering and Resource Utilization, Northeast Forestry University, Harbin, PR China
[d] Heilongjiang Provincial Key Laboratory of Ecological Utilization of Forestry-based Active Substances, Harbin, PR China

ARTICLE INFO

Keywords:
Docetaxel prodrug
Cascade targeting delivery
Metastatic bone cancer
Redox dual-responsive

ABSTRACT

Despite some advances in treating metastatic spread with docetaxel (DTX), it is almost not beneficial to treat metastatic bone cancer, a frequent lung, mammary, and prostate carcinoma complication. Therefore, a tumor-targeted platform was developed using DTX prodrug (DTX-S-DTX) enclosed inside docosahexaenoic acid-modified bovine albumin nanoparticles (DTX-S-DTX@DBNs). The biodistribution and drug release studies indicated that the DTX-S-DTX@DBNs features a cascade target delivery of DTX, from tumor vasculature to tumor tissue and then to a tumor cell. Furthermore, the DTX-S-DTX@DBNs exerted fewer side effects than that of DTX-S-DTX or DTX. Notably, the survival of the DTX-S-DTX@DBNs group (33.00 ± 2.55 d) was significantly longer compared with DTX-S-DTX group (26.71 ± 1.34 d, $p < 0.01$) or DTX group (25.43 ± 1.38 d, $p < 0.01$). The results indicated that the DTX-S-DTX@DBNs provide an exciting strategy for treating metastatic bone cancer, a significant clinical issue in lung and other cancers.

1. Introduction

Docetaxel (DTX), as an essential anticancer drug, is usually recommended first- or second-line treatment for lung, mammary, and prostate cancer [1]. Despite some advances in treating metastatic spread with DTX, it is almost not beneficial to treat metastatic bone cancer, a frequent complication of the lung, mammary, prostate carcinomas [2,3]. Moreover, DTX does not contribute a significant overall survival benefit for patients with bone metastases, leading to devastating and painful skeletal-related events [4]. Since nonspecific DTX may cause dose-limiting toxicity (lymphocytopenia or neutropenia) in patients with cancer, it is difficult to reach the minimal therapeutic concentration in metastatic bone cancer with low blood perfusion via intravenous administration [5,6]. So tumor passive targeting of human serum albumin (HSA) nanoparticles loading DTX (ABI-008) was attempted to discriminate DTX between healthy and neoplastic cells [7].

However, considering that most of the HSA binding proteins on the vascular endothelial cells of tumors are saturated by the endogenous HSA, and the rate-limiting step for tumor localization of albumin nanoparticles is extravasation from tumor vasculature, albumin needs to be tailored to targeting tumor vasculature [8,9]. Therefore, tumor vascular targeting agent (DTX@DBNs) was prepared by our group, and antitumor activities of the nanoparticles were investigated in our earlier work [10,11].

Unexpectedly, the phase II clinical trial of ABI-008 (Nab-Docetaxel) in patients with metastatic breast cancer had been terminated for its high toxicity, which cast a shadow on the clinical trial of DTX@DBNs in patients with metastatic cancer [7]. To avoid the unacceptable toxicity of sustained release of DTX from the nanoparticles, our group designed a tumor microenvironment responsive DTX dimeric prodrug (DTX-S-DTX) through a simple one step reaction [12].

Moreover, considering that tumor tissues are highly heterogeneous in accordance to redox potential difference, drug-drug conjugate via the monosulfide bond as a linkage can achieve redox dual-sensitive release of the drug in the tumor sites, ultimately alleviate the side effects of the drug in the blood circulation system [13]. Based on these, DTX-S-DTX was loaded in DBNs to obtain DTX-S-DTX@DBNs, designed to achieve a cascade target delivery of DTX from tumor vasculature to tumor tissue and then to tumor cells. Finally, the inhibiting metastatic bone cancer activities of the nanoparticles were investigated on an orthotopic mouse

* Corresponding author. Key Laboratory of Forest Plant Ecology, Northeast Forestry University, Hexing Road 26, 150040, Harbin, PR China.
** Corresponding author. Key Laboratory of Forest Plant Ecology, Ministry of Education, Northeast Forestry University, Harbin, PR China.
E-mail address: jiangsg2022@126.com (S. Jiang).

https://doi.org/10.1016/j.jddst.2022.103608
Received 17 March 2022; Received in revised form 27 June 2022; Accepted 14 July 2022
Available online 18 July 2022

model of bone metastasis.

2. Materials and methods

2.1. Materials

DTX was purchased from Yuancheng Gongchuang Technology Co., Ltd. (Wuhan, China). DHA was provided by Nu-Chek Prep Inc. (Elysian, MA, USA). BSA was obtained from Solarbio science & technology (Beijing, China). Thiodiglycolic anhydride (Tha), 1-hydroxybenzotriazole (HoBt) and 1-ethyl-3-(3-dimethylaminopropyl) carbodiimide hydrochloride (EDCI) were provided by Macklin Biochemical Co., Ltd. (Shanghai, China). Cyanine 5 NHS ester (Cy5-NHS) and fluorescein isothiocyanate (FITC) were purchased from Meilun Biotechnology Co., Ltd. (Dalian, China). HPLC-grade acetonitrile and methanol were provided by J&K Scientific Ltd. (Beijing, China). C57BL/6 mice were obtained from Vital River Laboratory Animal Technology Co., Ltd. (Beijing, China). LLC murine Lewis lung carcinoma cells, PC-3 human prostate cancer cells, A549 human lung adenocarcinoma cells, and H522 human lung adenocarcinoma cells were provided by the Cell Bank of the Chinese Academy of Sciences (Shanghai, China). All other materials were obtained from Aladdin (Shanghai, China).

2.2. Nanoparticles formulation and characterization

The synthetic route of DTX-S-DTX is shown in Fig. S1. In brief, Tha (33.03 mg, 0.25 mmol), EDCI (49.84 mg, 0.26 mmol), HoBt (35.13 mg, 0.26 mmol) and 10 μl triethylamine were dissolved in dry dichloromethane (10 ml). Then DTX (403.94 mg, 0.5 mmol) was slowly added to the reaction under nitrogen. After the reaction was stirred at room temperature for 24 h, the dichloromethane was evaporated under vacuum at 50 °C. Finally, the reaction product was purified by a silica gel column (chloroform: methanol = 27:2), and 235.97 mg product (96%) was obtained. The prodrug was confirmed by NMR spectroscopy (400 MHz ^{1}H NMR, Bruker Avance III, Switzerland) and MS spectrometry (AB SCIEX, Qtrap5500, USA).

The preparation and characterization method of the DTX-S-DTX@DBNs (DTX-S-DTX@BNs, DBNs, and BNs) was established consistently with our earlier studies [11]. In the biodistribution study, Cy5-NHS in DMSO (10 mg/ml) was added into the above DTX-S-DTX@BNs or DTX-S-DTX@DBNs solution at a Cy5: BSA ratio 2:1 for incubating 45 min at 25 °C in darkness. Then, the solutions were centrifugated at 1 × 10^5 g for 15 min. Lastly, Cy5 labeled nanoparticles were obtained.

2.3. Stability evaluation of DTX-S-DTX@DBNs

The stability of nanocarriers in serum is an important indicator to evaluate whether they can undergo long-circulation *in vivo* [14]. The DTX-S-DTX@DBNs were added to DMEM medium containing 10% FBS and incubated for 72 h at 37 °C, and then the changes of nanodrug size were recorded at 1, 2, 4, 6, 8, 10, 12, 18, 24, 36, 48 and 72 h, respectively. In addition, the storage stability of the DTX-S-DTX@DBNs was determined by particle size variation of lyophilized powders stored at 4 °C, 20 °C and 37 °C for 30 days, respectively.

2.4. In vitro drug release

The Taxotere®, DTX-S-DTX@BNs, and DTX-S-DTX@DBNs were diluted with PBS (pH 7.4), respectively. The obtained solution (5 ml, 0.5 mM) was put in Slide A-Lyzer™ dialysis cassettes (3.5 kDa), then the cassettes were stirred in a release media at 37 °C. At pre-determined time intervals, release media was withdrawn, and the same volume media was simultaneously supplied. The DTX content was determined by HPLC [7].

2.5. Redox triggered the release

The *in vitro* release profiles of DTX from DTX-S-DTX@DBNs were studied using a mixed solvent containing 30% ethanol in PBS buffer (pH 7.4, v/v) as release media. Then DTX-S-DTX@DBNs (200 μg, DTX-S-DTX equivalent) were stirred in 50 ml release media at 37 °C. At predetermined time intervals, 200 μl solution was withdrawn for HPLC analysis [7]. The release profiles in the presence of H2O2 or DTT were studied similarly, except for the addition of redox agents (5 mM H_2O_2 group, 10 mM H_2O_2 group, 5 mM DTT group, 10 mM DTT group) to the release media.

2.6. Cell studies

2.6.1. Cell culture

The cells were incubated in DMEM or RPMI1640 medium under a humidified 5% CO_2 atmosphere at 37 °C. All the media were supplemented with 10% (v/v) fetal bovine serum (FBS, Gibco) and 100 μg/ml streptomycin, and 100 U/ml penicillin (Gibco, Gaithersburg, MD, USA).

2.6.2. Cytotoxicity

Cells were seeded in 96-well plates (5000 cells per well) and were incubated for 18 h. Then the cells were treated or not for 48 h or 72 h at 37 °C. Then, 10 μl of MTT solution (0.5 mg/ml) was injected into the cultures. After incubation for 4 h, the supernatants were removed, and dimethyl sulfoxide was added at 200 μl per well. The absorbance values were then recorded by a spectrophotometer (Infinite 200 PRO, Tecan, Switzerland).

2.6.3. Cellular uptake analysis

In qualitative uptake studies, the PC-3 cells (1 × 10^5 cells) were seeded in six-well transparent plates for 24h and incubated with 1 μM FITC labeled nanoparticles for 2 h at 37 °C. After incubation, the cells were washed 3 times with PBS and observed by confocal laser scanning microscopy (Nikon, Tokyo, Japan).

In quantitative uptake studies, LLC cells (1 × 10^6 cells) were seeded in flasks for 48 h and incubated with 100 nM Cy5 labeled nanoparticles for 1 h at 37 °C. After incubation, the cells were detached from flasks. Then intracellular fluorescence intensity was measured by flow cytometry (Beckman, CytoFLEX, Suzhou, China).

2.7. Animal studies

6- to 7-week-old female C57BL/6 mice were provided with ad libitum water and standard laboratory mouse chow, and maintained at a temperature of 24 ± 1 °C on a 12 h light-dark cycle. All applicable international, national, and institutional guidelines for the care and use of animals were performed following a protocol approved by the Institutional Animal Care and Use Committee at the State Engineering Laboratory of Bio-Resources Eco-Utilization, Northeast Forestry University (20170601, June 1st, 2017).

2.7.1. Maximum tolerated dose determination

The C57BL/6 mice were randomly divided into the different groups (3 per group). The five doses (5, 10, 15, 20, and 25 μmol/kg) were selected to indicate the maximum tolerated dose (MTD). The animals were intravenously administered once daily for 7 days. The drugs' toxicity was assessed based on the monitoring of overall health, weight, and survival. The MTD was defined as the highest tested dose that caused neither >10% body-weight loss within 2 weeks of administration nor toxic mortality.

2.7.2. Biodistribution study

The LLC cells (2 × 10^6 cells per mouse) were inoculated subcutaneously to C57BL/6 mice in the right axillary region. Two weeks after implantation, the mice were intravenously injected with 50 mg/kg Cy5

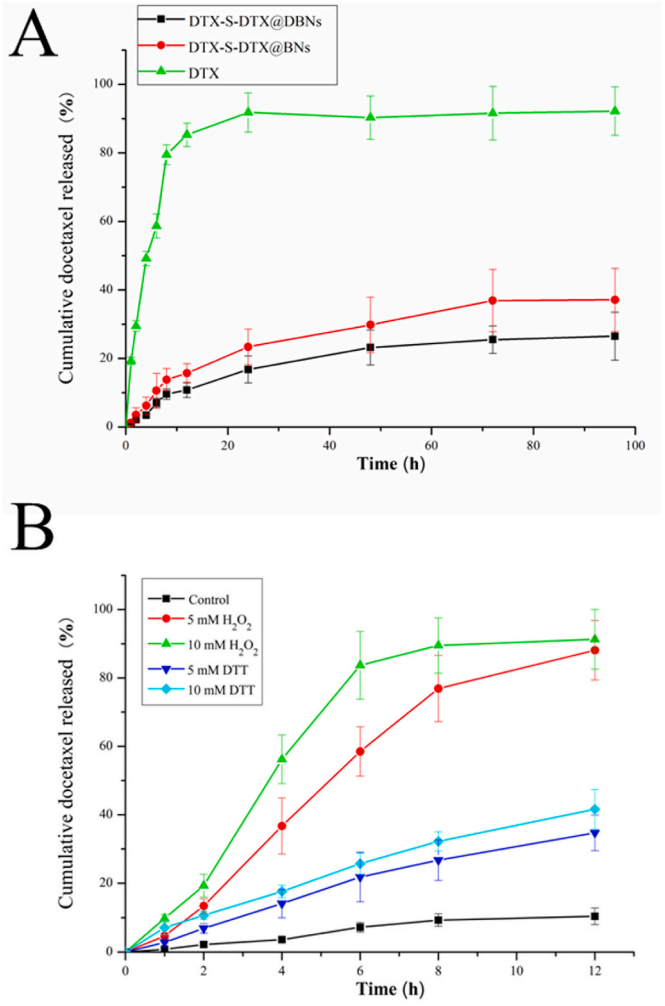

Fig. 1. *In vitro* drug release of the nanoparticles. (A) *In vitro* DTX release profile from nanoparticles or Taxoere® ($n = 3$); (B) *In vitro* DTX release profile from DTX-S-DTX@DBNs in the presence of various concentrations of H_2O_2 or DTT ($n = 3$).

Table 1
Cytotoxic effects of DTX-S-DTX@DBNs, n = 3.

Sample	IC50(μM)± SD, time = 48 h			
	DTX	DTX-S-DTX	DBNs	DTX-S-DTX@DBNs
LLC	0.037 ± 0.002	0.166 ± 0.013	>2000	0.198 ± 0.017
H522	0.005 ± 0.001	0.031 ± 0.002	>2000	0.045 ± 0.010
A549	0.050 ± 0.005	0.380 ± 0.024	>2000	0.542 ± 0.039
	IC50(μM)± SD, time = 72 h			
LLC	0.015 ± 0.001	0.065 ± 0.004	>2000	0.074 ± 0.006
H522	0.003 ± 0.001	0.019 ± 0.002	>2000	0.027 ± 0.003
A549	0.025 ± 0.005	0.152 ± 0.011	>2000	0.174 ± 0.012

labeled nanoparticles. After post-injection for 1 h, the fluorescence intensity (liver, kidney, lung, spleen, heart, tumor) was measured by IVIS®lumina Series III Spectrum Imaging System (Caliper Life Sciences, Inc., Hopkinton, MA).

2.7.3. *In vivo evaluation of antitumor efficacy and toxicity*

Ten C57BL/6 mice were randomly selected as a blank control, and the other mice were used intramedullary injection in the proximal tibia of the right limb with 10 μl LLC cells (1×10^6 cells/ml) after being anesthetized with ether. Then the mice were divided randomly into 5 groups: control group, positive control group injected with 5 μmol/kg DTX, 2.5 μmol/kg DTX-S-DTX group, 2.5 μmol/kg DTX-S-DTX@DBNs and 5 μmol/kg DTX-S-DTX@DBNs group. The mice were intravenously administered once daily for ten days on the second day after successful modeling. The tumor volume (TV), tumor inhibition rate (TIR, %), tumor inhibition index (TI), and relative tumor-inhibition index (RTI) was respectively calculated by the following formula: TV (mm^3) = 0.5 × Length (mm) × Width^2 (mm^2), TIR = ($TV_{Control\ group}$-$TV_{Treated\ group}$)/$TV_{Control\ group}$ × 100%, TI = Body weight/Tumor weight, and RTI = $TI_{Experimental\ group}/TI_{Control\ group}$. The default tumor density was 1 mg/mm^3.

2.7.4. *Radiographs*

At three weeks post-treatment, the mice's right hindlimb was imaged by BLX5 X-ray imaging equipment, and the bone injuries were recorded in the X-ray film (40 × 30 mm). Quantification of the radiolucent area in the tibia was obtained by Quantity One Analysis Software. X-ray film development was performed according to the protocol.

2.7.5. *Histology*

At three weeks post-treatment, the harvested tibias were fixed in formalin and decalcified in EDCI solution. The samples were then dehydrated, embedded and cut into sections. After being deparaffinized, the sections were stained with HE. Finally, the sections were observed using a light microscope.

2.8. *Statistical analysis*

Numerical data are expressed as the mean ± standard deviation (SD). Statistical significance was determined by one-way analysis of variance (ANOVA) with posthoc Newman-Keuls (SPSS software).

3. Results and discussion

3.1. *Synthesis and characterization of DTX-S-DTX*

DTX-S-DTX was synthesized from thiodiglycolic anhydride and DTX by esterification via two single thioester bonds (Fig. S1). The 2′-hydroxyl of DTX was used to couple thiodiglycolic anhydride because the esterification of the 2′-hydroxyl group is more accessible [15]. The yield of the reaction was 52.28%. ESI/MS and ^{1}H NMR demonstrated the successful synthesis of DTX-S-DTX C–S bond of DTX-S-DTX with a theoretical molecular weight of 1729.9 is more comfortable to break, so DTX-S-DTX firstly formed fragment ions (M_1:848.3534, M_2:881.5445). As exhibited in Fig. S2A, the peak with the *m/z* value of 943.9890 indicates M-DTX-H + Na^+ (M-807.88-1+23), the peak with the *m/z* value of 927.6611 indicates M-DTX-H_2O + Na^+ (M-807.88-18 + 23), the peak of *m/z* 830.3341 indicates M_1-H_2O (M_1-18). There were no peaks for the ^{1}H NMR spectrum of DTX at 3.5–3.9 δ (ppm), but the ^{1}H NMR spectrum of DTX-S-DTX was shown in Fig. S2B, where the appearance of peaks at δ/ppm 3.65 (m, 4H, $-CH_2SCH_2$) indicated the existence of 2 DTX and S-bond in the monosulfide-linked DTX-DTX conjugate. Furthermore, the peaks (7, 10 and 2′ proton) of ^{1}H NMR spectrum of DTX appeared at 4.26, 5.22, and 4.62 δ (ppm) respectively, and peaks for ^{1}H NMR spectrum of DTX-S-DTX appeared at 4.26 and 5.22 δ (ppm) but disappeared at 4.62 δ (ppm), which indicated 2′-hydroxyl of DTX was coupled to thiodiglycolic anhydride [15].

3.2. *Preparation and characterization of nanoparticles*

Due to the limited solubility of DTX-S-DTX in a mixed solvent, the maximum concentration of DTX-S-DTX in the mixed solvent (3 mg/ml) was selected as the optimal condition of DTX-S-DTX concentration. The other optimal conditions (DHA-BSA concentration: 9 mg/ml, the ratio of water to organic phase: 16:1, the homogenate speed: 6000 rpm, the homogenate time: 6 min, the homogenization pressure: 800 bar and the homogenization times: 7) were determined by a single-factor method.

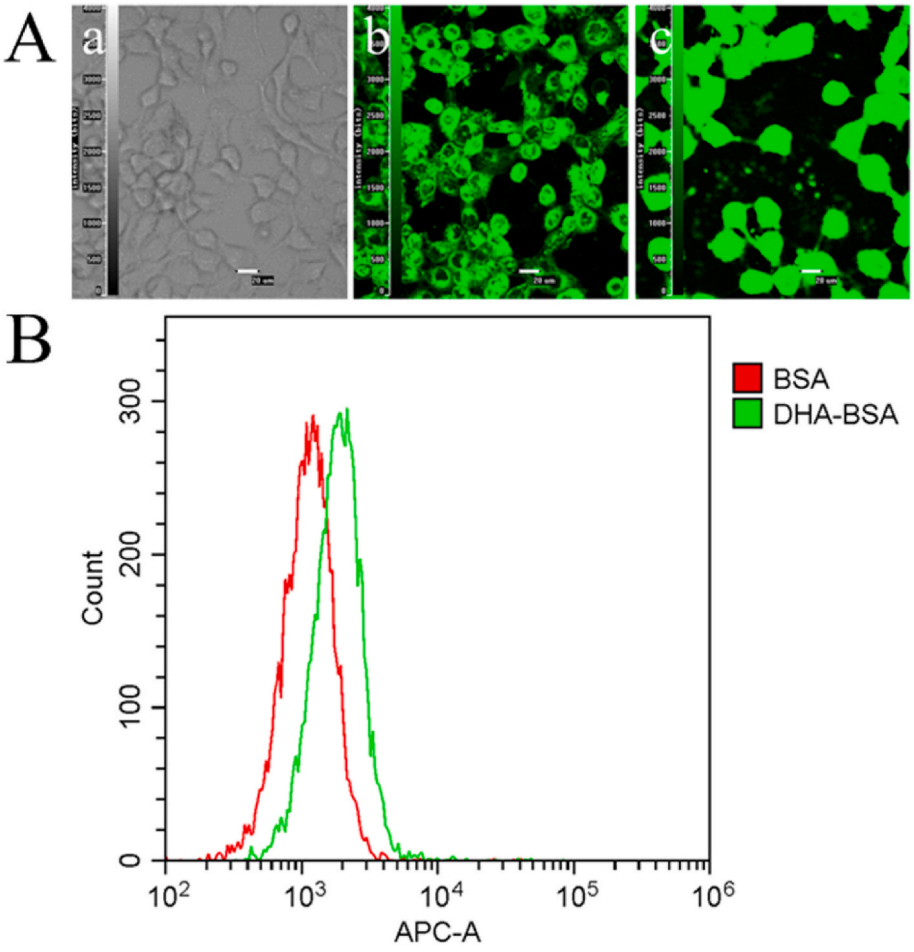

Fig. 2. Cellular uptake assay. (A) Confocal laser scanning microscopy analysis of PC-3 cells treated with (a) no drug (magnification: 200x), (b) DTX-S-DTX@BNs (magnification: 200x), (c) DTX-S-DTX@DBNs (magnification: 400x); (B) Flow cytometry analysis of LLC cells treated with Cy5-labeled DTX-S-DTX@BNs or DBNs. DHA-BSA: Cy5-labeled DTX-S-DTX@DBNs; BSA: Cy5-labeled DTX-S-DTX@BNs.

DTX-S-DTX@DBNs was found to be non-spherical shaped (Fig. S3A), and there were oligomers of the DTX-S-DTX@DBNs due to linking the DHA with the fatty acid-binding sites of BSA among the different nanoparticles [16,17]. Non-spherical DBNs with high aspect ratios could marginate more readily than spherical BNs and establish firm adhesion to tumor vessel walls, so DTX-S-DTX@DBNs could possess the advantage of extravasation from tumor vasculature [18].

The mean diameter of particles of BNs, DBNs, DTX-S-DTX@BNs, and DTX-S-DTX@DBNs was 87.8 ± 8.9 nm, 96.8 ± 10.3 nm, 97.9 ± 11.5 nm, and 101.8 ± 12.4 nm, respectively. Although the mean SEM diameter of the nanoparticles was larger than the opening in the bone marrow fenestrations (170 nm), the mean hydrodynamic diameter of the nanoparticles was significantly below the opening fenestrations, which indicated the nanoparticles could be delivered to tumors in the bone marrow [6]).

The zeta potential of BPs, DBNs, DTX-S-DTX@BNs, and DTX-S-DTX@DBNs was −17.61 ± 0.20 mV, −17.50 ± 2.77 mV, −20.23 ± 1.24 mV, −21.12 ± 1.51 mV, respectively, so the nanoparticles with negative surface properties can possess excellent stability in suspension and a long blood circulation effect *in vivo* [18]. Nanodrugs with suitable particle size and good stability in solution are very favorable for enrichment at tumor sites through EPR effect [19]. As shown in Fig. S4A, the particle size change of DTX-S-DTX@DBNs was less than 15% after incubation in DMEM medium containing 10% FBS for 72 h. This indicates that the DTX-S-DTX@DBNs has excellent anti-protein adsorption ability and good stability in serum. This may be due to the fact that the surface of DTX-S-DTX@DBNs carries negative charge, which makes it easier for the carrier particles to escape from protein capture and facilitates the long-circulation in the blood. In Fig. S4B, there was no significant change in particle size after 30 d of storage in 4 °C, 20 °C and 37 °C, respectively. This also demonstrates again the excellent storage stability of the DTX-S-DTX@DBNs [7].

Due to the higher lipophilicity of DHA-BSA compared with BSA, the drug-loading capacity of DHA-BSA was enhanced by the stronger binding affinity between DTX-S-DTX and the hydrophobic segment [18]. Hence, the loading efficiency of DTX-S-DTX@DBNs reached up to 7.8% ± 1.4%, and the drug entrapment efficiency up to 84.6% ± 4.3% was achieved. The content of DHA in DTX-S-DTX@DBNs was 4.0% ± 1.2%, which implied about 9 molecules of DHA were conjugated to 1 molecule of BSA [11].

The characteristic peak ($2\theta = 10.71°, 12.15°, 13.57°, 17.14°, 19.29°$) and melting point (216.07 °C) of DTX-S-DTX in the nanoparticles disappeared (Figs. S3B–C), which indicated that DTX-S-DTX was in an amorphous or disordered crystalline phase.

3.3. *In vitro* drug release

A burst release of DTX from Taxotere® was found to compare the other two nanoparticles. At the first 96 h, the DTX in DTX-S-DTX@BNs released faster than DTX-S-DTX@DBNs. For the DTX-S-DTX@DBNs, DTX released rapidly with a release of about 1% per hour at the first 8 h. In the following hours, it slowed down, especially in the last 24 h with a release of 1%. The cumulative release of DTX-S-DTX@DBNs (26.5% ± 7.0%) was less than Taxotere® (92.2% ± 7.1%) or DTX-S-

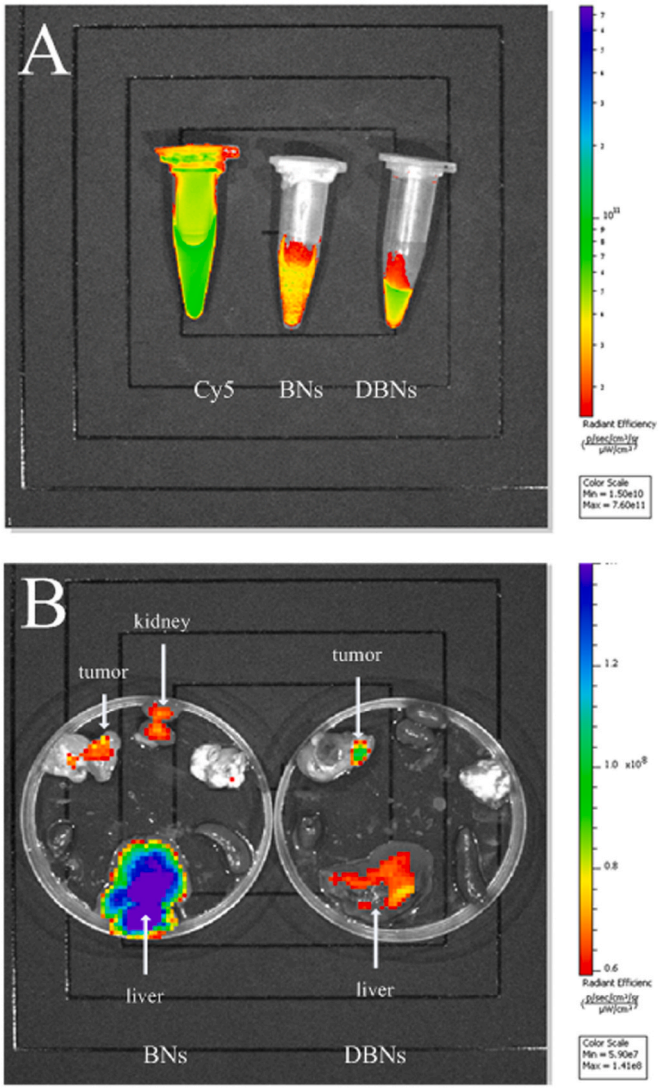

Fig. 3. The mice were observed by Spectrum Imaging System. (a) Cy5 solution and Cy5-labeled DTX-S-DTX@DBNs or DTX-S-DTX@BNs. (b) Ex vivo biodistribution of Cy5-labeled DTX-S-DTX@DBNs or DTX-S-DTX@BNs at 1h. DBNs: Cy5-labeled DTX-S-DTX@DBNs; BNs: Cy5-labeled DTX-S-DTX@BNs; H: high fluorescence intensity, M: middle fluorescence intensity, L: low fluorescence intensity.

DTX@BNs (37.1% ± 9.2%) after the 96 h (Fig. 1A). The results indicated that the DTX-S-DTX@DBNs were released in a sustained manner and could have prolonged circulation time to increase the passive accumulation in tumor tissues [18].

3.4. Redox triggered release

Only 10.4% of DTX was released from DTX-S-DTX@DBNs in 12 h without H_2O_2 or DTT (Fig. 1B). In comparison, in the release medium containing 5 mM H_2O_2 or 10 mM H_2O_2, 88.1% or 91.3% of DTX were released in 12 h, respectively. In the release medium containing 5 mM DTT or 10 mM DTT, 34.7% or 41.6% of DTX were released in 12 h, respectively. DTX-S-DTX@DBNs exhibited redox-responsive drug delayed release in the presence of H_2O_2 or DTT [15].

The results indicated that the DTX-S-DTX@DBNs could achieve sensitive release of DTX in tumor redox environments. Therefore, the DTX-S-DTX@DBNs might avoid the failure of clinical trials of PTX-DHA for the inefficient release of paclitaxel (PTX) from PTX-DHA [7].

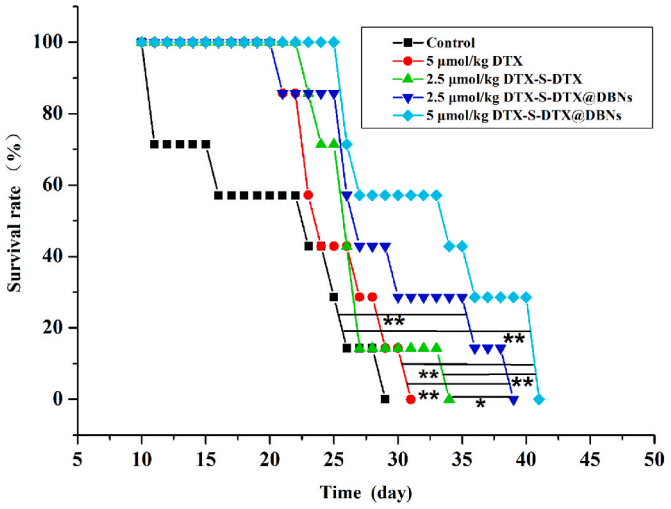

Fig. 4. Kaplan-Meier survival curves of the mice transplanted LLC cells after treatment with saline, 5 μmol/kg DTX, 2.5 μmol/kg DTX-S-DTX, 2.5 μmol/kg DTX-S-DTX@DBNs, and 5 μmol/kg DTX-S-DTX@DBNs. $n = 20$/group. $^{*}p < 0.01$ vs.control, $^{**}p < 0.01$ vs. 5 μmol/kg DTX group, $^{\#}p < 0.05$ vs. 2.5 μmol/kg DTX-S-DTX group, $^{\#\#}p < 0.01$ vs. 2.5 μmol/kg DTX-S-DTX group.

3.5. Cytotoxicity

The IC_{50} values of DTX-S-DTX and DTX-S-DTX@DBNs were more than that of DTX for the tumor cells (Table 1). The results demonstrated that DTX-S-DTX and DTX-S-DTX@DBNs attenuated cytotoxicity compared with DTX, so the dosage of DTX-S-DTX@DBNs can be increased for their sustained release of the DTX-S-DTX in the blood. Furthermore, the IC_{50} values of DTX-S-DTX were more than that of DTX for the tumor cells. Considering that the cytotoxic activity of DTX-S-DTX mainly depends on the liberation of active DTX, so the compromised *in vitro* cytotoxicity of DTX-S-DTX indicated that DTX-S-DTX with a large molecular size accumulated less in the tumor cells in comparison with DTX [20,21].

3.6. Cellular uptake

A significant fluorescence difference between DTX-S-DTX@BNs and DTX-S-DTX@DBNs can be observed, and the DTX-S-DTX@DBNs has the higher target effect (Fig. 2A). Furthermore, the uptake efficiency of DTX-S-DTX@DBNs (2206.9) was about 1.5 fold higher than DTX-S-DTX@BNs (1421.7) (Fig. 2B). Thus it is speculated that phosphatidylethanolamine was highly expressed in the LLC cells.

3.7. Maximum tolerated dose determination

The MTD of DTX-S-DTX (10 μmol/kg) was equal to that of DTX (10 μmol/kg), but two DTX molecules could be released from one DTX-S-DTX molecule, which indicated that DTX-S-DTX could be easier to reach the therapeutic concentration at the lesions in comparison with DTX. Moreover, the MTD of DTX-S-DTX@DBNs (15 μmol/kg) was 1.5 fold higher than DTX-S-DTX (10 μmol/kg), which indicated DTX-S-DTX@DBNs could be easier to reach the minimal therapeutic concentration at the metastatic bone cancer in comparison with DTX-S-DTX.

3.8. Biodistribution study

The DTX-S-DTX@BNs mainly accumulated in the liver, and weak fluorescence intensity could be observed in the tumor and kidney for the group of DTX-S-DTX@BNs after post-injection for 1h. By contrast, the DTX-S-DTX@DBNs mainly accumulated in the tumor, and weak fluorescence intensity could be observed in the liver for the group of DTX-S-

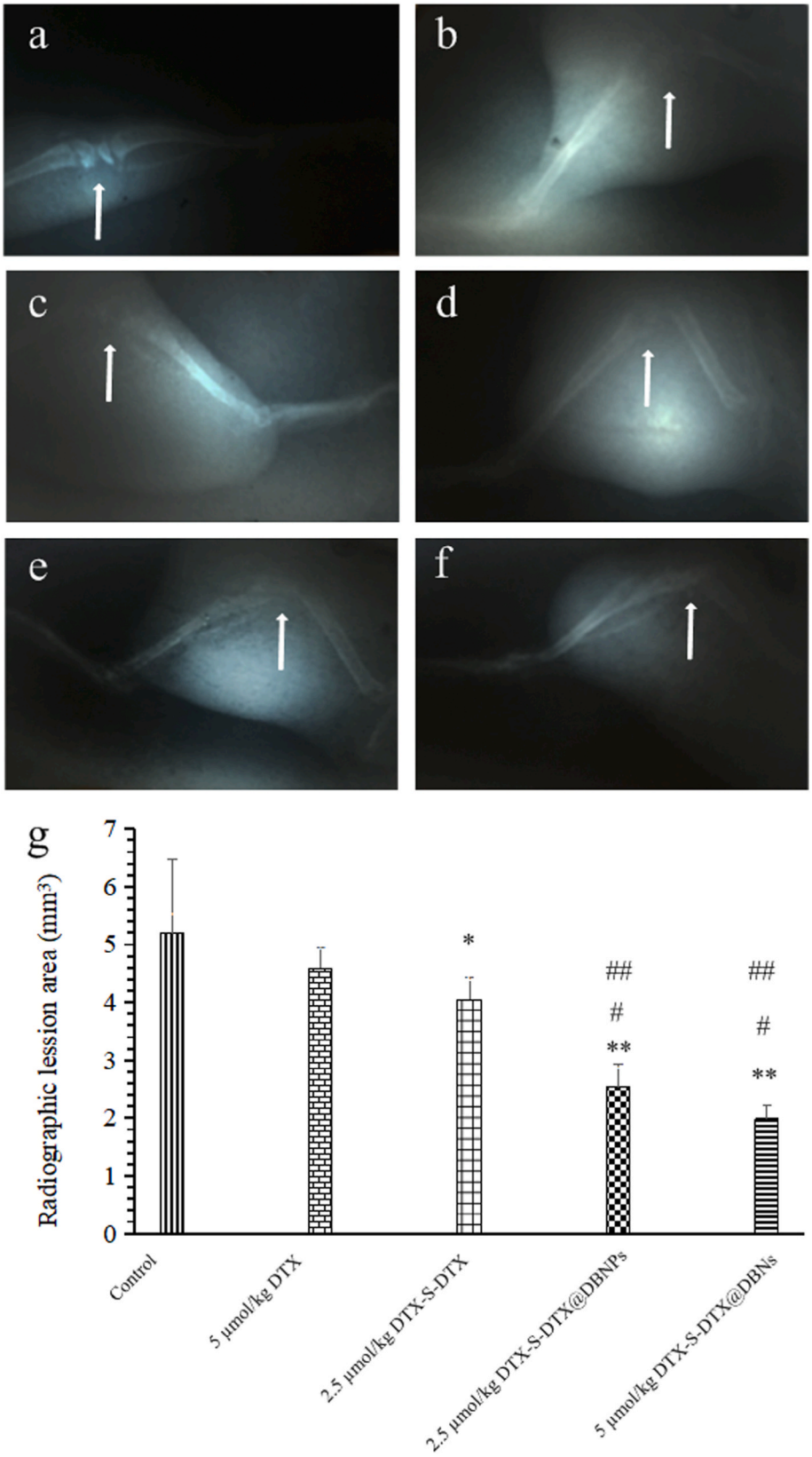

Fig. 5. X-ray radiography images of the five model groups show osteolytic lesions. Three weeks after the initial injection, the mice were imaged by X-ray equipment and representative pictures from the (a) blank control, (b) negative control, (c) 5 μmol/kg DTX, (d) 2.5 μmol/kg DTX-S-DTX, (e) 2.5 μmol/kg DTX-S-DTX@DBNs, and (f) 5 μmol/kg DTX-S-DTX@DBNs groups are presented. Magnification, ×1. (g) areas of osteolytic bone metastases of the tibia were quantified for LLC cells by Quantity One analysis software. $n = 20$/group. $^{*}p < 0.05$ vs. negative control group, $^{**}p < 0.01$ vs. negative control group, $^{\#}p < 0.01$ vs. 5 μmol/kg DTX group, $^{\#\#}p < 0.05$ vs. 2.5 μmol/kg DTX-S-DTX group.

DTX@DBNs. Furthermore, the fluorescence intensity of DTX-S-DTX@DBNs in the tumor was more potent than that of DTX-S-DTX@BNs (Fig. 3). These results showed that DTX-S-DTX@DBNs could achieve delivery DTX from tumor vasculature to tumor tissue and have a much higher tumor-targeting capacity than DTX-S-DTX@BNs.

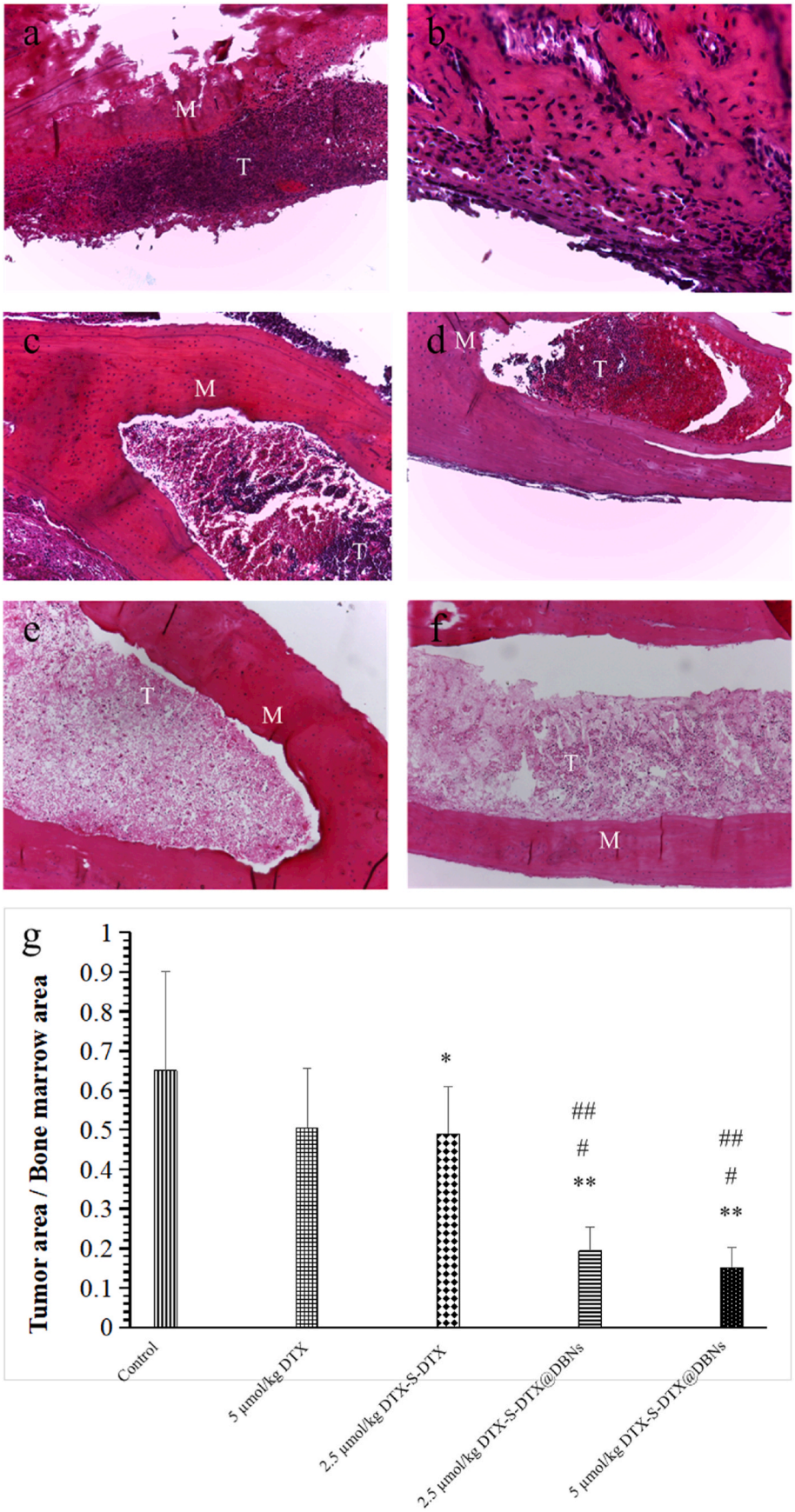

Fig. 6. The light microscopy images showed HE-stained bones of the mice implanted with LLC cells. (a) Control (magnification: 100x), (b) Control (magnification: 400x), (c) 5 μmol/kg DTX (magnification: 100x), (d) 2.5 μmol/kg DTX-S-DTX (magnification: 100x), (e) 2.5 μmol/kg DTX-S-DTX@DBNs (magnification: 100x), (f) 5 μmol/kg DTX-S-DTX@DBNs (magnification: 100x) and (g) Tumor areas were quantified by Image-Pro Plus software. $n = 20$/group. $^{*}p < 0.05$ vs. control group, $^{**}p < 0.01$ vs. control group, $^{\#}p < 0.01$ vs. 5 μmol/kg DTX group, $^{\#\#}p < 0.01$ vs. 2.5 μmol/kg DTX-S-DTX group.

3.9. In vivo evaluation of antitumor efficacy and toxicity

The five-year survival of lung cancer patients with bone metastases is the lowest among significant cancer [4]. Furthermore, it is easy to ignore nanoparticles' false positive therapeutic effect in the commonly used tumor xenografts model [22]. Therefore, the therapeutic efficacy of the nanoparticles against metastatic bone cancer was investigated in an autograft bone metastasis model of lung cancer.

The survival in the DTX@BNs group did not increase significantly compared with the DTX group [11]. Furthermore, the survival in the DTX-S-DTX@BNs group against metastatic bone cancer did not increase significantly compared with the DTX-S-DTX group (data not shown), so the DTX-S-DTX@BNs group was not selected as a treatment group in the following experiment.

The RTI of 2.5 μmol/kg DTX-S-DTX@DBNs (3.5 ± 0.4) group or 5 μmol/kg DTX-S-DTX@DBNs group (4.3 ± 0.5) was significantly higher than that of DTX-S-DTX group (2.8 ± 0.4) or DTX group (2.0 ± 0.2), which indicated that DTX-S-DTX@DBNs exerted fewer side effects than that of DTX-S-DTX or DTX ($p < 0.01$ vs. 5 μmol/kg DTX group or 5 μmol/kg DTX-S-DTX group). The cytotoxicity of DTX-S-DTX was less than that of DTX. However, the TIR of 2.5 μmol/kg DTX-S-DTX group (64.9% ± 15.8%) was significantly higher than that of 5 μmol/kg DTX group (51.0% ± 7.3%), which indicated DTX-S-DTX could achieve selective release of DTX in tumor tissue ($p < 0.01$ vs. 5 μmol/kg DTX group). Moreover, the TIR of 2.5 μmol/kg DTX-S-DTX@DBNs (69.9% ± 11.2%) group or 5 μmol/kg DTX-S-DTX@DBNs group (74.6% ± 10.6%) was significantly higher than that of 5 μmol/kg DTX group or 2.5 μmol/kg DTX-S-DTX group ($p < 0.01$ vs. 5 μmol/kg DTX group, $p < 0.05$ vs. 5 μmol/kg DTX-S-DTX group). Hence, the designed nanoparticles could be safely applied in the clinic treatment of bone metastases.

The mean survival for the animals in the saline group, positive control group (5 μmol/kg DTX), 2.5 μmol/kg DTX-S-DTX group, 2.5 μmol/kg DTX-S-DTX@DBNs group, and 5 μmol/kg DTX-S-DTX@DBNs group was 19.86 ± 2.96 d, 25.43 ± 1.38 d, 26.71 ± 1.34 d, 29.29 ± 2.37 d, and 33.00 ± 2.55 d, respectively (Fig. 4). The results demonstrated that DTX-S-DTX@DBNs exhibits a higher inhibitory activity against metastatic bone cancer than DTX-S-DTX or DTX.

3.10. Radiographs

At 21 days post-treatment, a total of 20, 17, 14, 10 and 6 mice were subjected to severe tibia injury in the saline group, 5 μmol/kg DTX group, 2.5 μmol/kg DTX-S-DTX group, 2.5 μmol/kg DTX-S-DTX@DBNs group and 5 μmol/kg DTX-S-DTX@DBNs group, respectively (Fig. 5; white arrow). Except for the tibias in the blank group that were intact, the others in each group were variously damaged. The results indicated that DTX-S-DTX@DBNs exhibits a more potent inhibitory effect against metastatic malignant lesions in bone in comparison with DTX-S-DTX or DTX.

3.11. Histology

As shown in Fig. 6, there were plenty of tumor cells (T region) in the control group, 5 μmol/kg DTX group, and 2.5 μmol/kg DTX-S-DTX group, moreover the cortex of the tibia (M region) had been severely eroded. However, the cortical endosteum (M region) in the DTX-S-DTX@DBNs groups had been slightly eroded, especially in 5 μmol/kg DTX-S-DTX@DBNs group was nearly intact. The results indicated the DTX-S-DTX@DBNs could deliver the DTX to the bone-metastatic tumor cells in the bone marrow. Since phosphatidylethanolamine, which is the receptor for DHA, is overexpressed in tumor vascular endothelium, DHA can be better bound to phosphatidylethanolamine in tumor vascular endothelium and thus taken up by malignant cells. In our designed nano-targeted delivery system (DTX-S-DTX@DBNs), coupling DHA with albumin as a carrier for the prodrug DTX-S-DTX allows the drug to achieve its targeted enrichment effect when passing through the tumor vessel [10]. Specifically, the transcytosis mechanism mediated by denatured albumin receptors on the surface of vascular endothelial cells and the DTX uptake mechanism of cancer cells mediated by SPARC in the tumour strom is presumed [23]. Finally excess GSH and ROS are produced in tumor cells, then the tumor tissue will be created into a high redox microenvironment. This allows the disulfide bonds in the precursor drug (DTX-S-DTX) that accumulates in the tumor to break rapidly and release double the amount of DTX, thus achieving the anti-tumor target [20].

4. Conclusions

According to the strategy of prodrug and drug delivery systems, DTX-S-DTX@DBNs were successfully prepared by our group. *In vivo*, the smart DTX-S-DTX@DBNs had improved the selectivity of chemotherapeutics, which reflected the enormous potential of the DTX-S-DTX@DBNs in metastatic bone cancer therapy.

Author's contributions

Shougang Jiang, Yuangang Zu and Liang Wei conceived, designed the study and wrote manuscript. Liang Wei and Dong Zhang performed the preparation of raw materials, process optimization. Liang Wei and Bin Xiong completed *in vivo* and *in vitro* activity experiments. Shougang Jiang, Liang Wei and Siyan Zhang processed and analyzed the experimental data and plotted them. All authors read and approved the manuscript.

Sources of support

This study was supported by the Science Foundation of Heilongjiang Province, China (grant no. H2018001), the Fundamental Research Funds for the Central Universities (grant no. 2572018BU03) and the Heilongjiang Postdoctoral (grant no. LBH-Z10282).

Declaration of competing interest

We declare that we have no financial and personal relationships with other people or organizations that can inappropriately influence our work, there is no professional or other personal interest of any nature or kind in any product, service and/or company that could be construed as influencing the position presented in, or the review of, the manuscript entitled.

Data availability

Data will be made available on request.

Appendix A. Supplementary data

Supplementary data to this article can be found online at https://doi.org/10.1016/j.jddst.2022.103608.

References

[1] R. da Costa, G.F. Passos, N.L.M. Quintão, E.S. Fernandes, J.R.L.C.B. Maia, M. M. Campos, et al., Taxane-induced neurotoxicity: pathophysiology and therapeutic perspectives, Br. J. Pharmacol. 177 (2020) 3127–3146.
[2] M.A. Isaac, N.T. Madison, B.B. Shannon, S. Blanka, Targeted nanomedicine to treat bone metastasis, Pharmaceutics 10 (2018) 205–226.
[3] A. Argentiero, A.G. Solimando, O. Brunetti, A. Calabrese, F. Pantano, M. Iuliani, et al., Skeletal metastases of unknown primary: biological landscape and clinical overview, Cancers 11 (2019) 1270–1287.
[4] H. Murakami, T. Yamanaka, T. Seto, K. Sugio, I. Okamoto, T. Sawa, et al., Phase II study of zoledronic acid combined with docetaxel for non-small-cell lung cancer: west Japan Oncology Group, Cancer Sci. 105 (2014) 989–995.
[5] I. Ojima, X. Wang, Y. Jing, C. Wang, Quest for efficacious next-generation taxoid anticancer agents and their tumor-targeted delivery, J. Nat. Prod. 81 (2018) 703–721.

[6] I.M. Adjei, B. Sharma, C. Peetla, V. Labhasetwar, Inhibition of bone loss with surface-modulated, drug-loaded nanoparticles in an intraosseous model of prostate cancer, J. Contr. Release 32 (2016) 83–92.
[7] X. Tang, G. Wang, R. Shi, K. Jiang, L. Meng, H. Ren, et al., Enhanced tolerance and antitumor efficacy by docetaxel-loaded albumin nanoparticles, Drug Deliv. 23 (2016) 2686–2696.
[8] Z. Luo, H. Tian, L. Liu, Z. Chen, R. Liang, Z. Chen, et al., Tumor-targeted hybrid protein oxygen carrier to simultaneously enhance hypoxia-dampened chemotherapy and photodynamic therapy at a single dose, Theranostics 8 (2018) 3584–3596.
[9] D.B. Kirpotin, D.C. Drummond, Y. Shao, M.R. Shalaby, K. Hong, U.B. Nielsen, et al., Antibody targeting of long-circulating lipidic nanoparticles does not increase tumor localization but does increase internalization in animal models, Cancer Res. 66 (2006) 6732–6740.
[10] J.H. Stafford, P.E. Thorpe, Increased exposure of phosphatidylethanolamine on the surface of tumor vascular endothelium, Neoplasia 13 (2011) 299–308.
[11] Y. Zu, Y. Hu, X. Yu, S. Jiang, Docetaxel-loaded bovine serum albumin nanoparticles conjugated docosahexaenoic acid for inhibiting lung cancer metastasis to bone, Anti Cancer Agents Med. Chem. 17 (2017) 542–551.
[12] H. Kenmotsu, C.K. Imamura, A. Ono, S. Omori, K. Nakashima, K. Wakuda, et al., The effects of advanced age and serum α1-acid glycoprotein on docetaxel unbound exposure and dose-limiting toxicity in cancer patients, Br. J. Clin. Pharmacol. 83 (2017) 2416–2425.
[13] Q. Song, X. Wang, Y. Wang, Y. Liang, Y. Zhou, X. Song, et al., Reduction responsive self-assembled nanoparticles based on disulfide-linked drug-drug conjugate with high drug loading and antitumor efficacy, Mol. Pharm. 13 (2016) 190–201.
[14] G.L. Ma, X. Du, J.P. Zhu, F. Xu, H. Yu, J. Li, Multi-functionalized dendrimers for targeted co-delivery of sorafenib and paclitaxel in liver cancers, J. Drug Deliv. Sci. Technol. 63 (2021), 102493.
[15] W. Wei, C. Luo, J. Yang, B. Sun, D. Zhao, Y. Liu, et al., Precisely albumin-hitchhiking tumor cell-activated reduction/oxidation responsive docetaxel prodrugs for the hyperselective treatment of breast cancer, J. Contr. Release 285 (2018) 187–199.
[16] F.F. An, X.H. Zhang, Strategies for preparing albumin-based nanoparticles for multifunctional bioimaging and drug delivery, Theranostics 7 (2017) 3667–3689.
[17] J.A. Hamilton, NMR reveals molecular interactions and dynamics of fatty acid binding to albumin, Biochim. Biophys. Acta 1830 (2013) 5418–5426.
[18] H. Ye, Z. Shen, L. Yu, M. Wei, Y. Li, Manipulating nanoparticle transport within blood flow through external forces: an exemplar of mechanics in nanomedicine, Proc. Math. Phys. Eng. Sci. 474 (2018) 20170845–20170860.
[19] E. Ribeiro, F. Marques, L. Gano, J.D.G. Correia, I. Santos, C. Fernandes, Docetaxel-loaded block copolymer micelles labeled with Re-188 for combined radiochemotherapy, J. Drug Deliv. Sci. Technol. 60 (2020), 101898.
[20] C. Luo, J. Sun, D. Liu, B. Sun, L. Miao, S. Musetti, et al., Self-assembled redox dual-responsive prodrug-nanosystem formed by single thioether-bridged paclitaxel-fatty acid conjugate for cancer chemotherapy, Nano Lett. 16 (2016) 5401–5408.
[21] S. Chillistone, J. Hardman, Factors affecting drug absorption and distribution, Anaesth. Intensive Care Med. 12 (2011) 151–155.
[22] D. Rosenblum, N. Joshi, W. Tao, J.M. Karp, D. Peer, Progress and challenges towards targeted delivery of cancer therapeutics, Nat. Commun. 9 (2018) 1410–1422.
[23] Y. Ishima, T. Maruyama, M. Otagiri, V.T.G. Chuang, T. Ishida, The new delivery strategy of albumin carrier utilizing the interaction with albumin receptors, Chem. Pharm. Bull. 70 (2022) 330–333.